UNIVERSITY OF LODZ

FACULTY OF CHEMISTRY

Department of Theoretical and Structural Chemistry

Author's review of her research

(annex 2b)

Lilianna Chęcińska

1. First name and surname

Lilianna Chęcińska (née Świerczyńska)

2. Education, scientific diploma and degrees

- June 16th, 1999 – MSc degree, Faculty of Physics and Chemistry, University of Lodz

  MSc dissertation: Crystal structure determination of *O*-phenyl (triphenylphosphoniomethyl)phosphonate phenol solvate using X-ray diffraction analysis.
  Supervisor: Dr. Tomasz A. Olszak
  Reviewer: Prof. Dr. Mieczysław Grabowski

- May 28th, 2003 – PhD degree, Faculty of Physics and Chemistry, University of Lodz

  PhD dissertation: Crystal and molecular structures of new derivatives of *N*,*N*'-substituted phosphonylated thiourea.
  Supervisor: Prof. Dr. Maria Bukowska-Strzyżewska (Technical University of Lodz)
  Reviewers: Prof. Dr. Zofia Kosturkiewicz (University A. Mickiewicza w Poznaniu)
  Dr. hab. Wojciech Wolf (Technical University of Lodz)

3. Employment

- since 2003 – Associate Professor, Department of Theoretical and Structural Chemistry, Faculty of Chemistry, University of Lodz
- 2002 – 2003 – Assistant, Department of Crystallography and Crystal Chemistry, Faculty of Physics and Chemistry, University of Lodz
- 1999 – 2003 – PhD student, Faculty of Physics and Chemistry, University of Lodz

4. Scientific achievements submitted for the habilitation procedure

As an achievement resulting from Article 16, section 2 of the Act on Academic Degrees and Titles and about Degrees and Titles in the Field of Fine Arts of March 14, 2003 (Dz. U. No 65/2003, item 595, with subsequent amendments) 8 of scientific publications are designed [H1-H8].

4.1. Title of scientific achievements

Characterization of chemical bonding and non-covalent interactions on the basis of theoretical and/or experimental electron-density distribution.

4.2. List of publications comprising the scientific achievements

H1 Lilianna Chęcińska, Sławomir J. Grabowski*
F-H···F-C hydrogen bonds -The influence of hybridization of carbon atom connected with F-acceptor on their properties.
Chemical Physics (2006). 327, 202-208.

H2 Lilianna Chęcińska, Stefan Mebs, Christian B. Hübschle, Diana Förster, Wolfgang Morgenroth, Peter Luger*
Reproducibility and transferability of topological data: experimental charge density study of two modifications of *L*-alanyl-*L*-tyrosyl-*L*-alanine.
Organic & Biomolecular Chemistry (2006). 4, 3242-3251.

H3 Da'san M.M. Jaradat, Stefan Mebs, Lilianna Chęcińska, Peter Luger*
Experimental charge density of sucrose at 20 K: Bond topological, atomic and intermolecular quantitative properties.
Carbohydrate Research (2007). 342, 1480-1489.

H4 Lilianna Chęcińska, Sergey I. Troyanov, Stefan Mebs, Christian B. Hübschle, Peter Luger*
Examination of intermolecular electronic interactions in the crystal structure of $C_{60}(CF_3)_{12}$ by experimental electron density determination.
Chemical Communications (2007). 4003-4005.

H5 Lilianna Chęcińska,* Simon Grabowsky, Magdalena Małecka, Agnieszka J. Rybarczyk-Pirek, Andrzej Jóźwiak, Carsten Paulmann, Peter Luger
Experimental and theoretical electron density study of three isoindole derivatives: topological and Hirshfeld surface analysis of weak intermolecular interactions.
Acta Crystallographica (2011). B67, 569-581.

H6 Lilianna Chęcińska,* Wolfgang Morgenroth, Carsten Paulmann, Dylan Jayatilaka, Birger Dittrich
A comparison of electron density from Hirshfeld-atom refinement, X-ray wavefunction refinement and multipole refinement on three urea derivatives.
CrystEngComm (2013). 15, 2084-2090.

H7 Lilianna Chęcińska,* Stefan Mebs, Borys Ośmiałowski, Anna Zakrzewska, Krzysztof Ejsmont, Miroslav Kohout
Tuning the electronic properties of the dative N–B bond with associated O–B interaction – the electron localizability indicator from X-ray wavefunction refinement.
ChemPhysChem (2016). DOI: 10.1002/cphc.201600223.

H8 Maria Kasprzak,* Małgorzata Fabijańska, Lilianna Chęcińska, Leszek Szmigiero, Justyn Ochocki
New look on 3-hydroxyiminoflavanone and its palladium(II) complex: crystallographic and spectroscopic studies, theoretical calculations and cytotoxic activity.
Molecules (2016). 21, 455.

4.3. Description of the scientific aim and results achieved

Introduction

My scientific adventure with crystallography began in 1998 during the preparation of my Master's thesis, during which I crystallized substances, choose crystals for study and participated in X-ray data collection. The following years saw me continuing my X-ray studies as a PhD student in the Faculty of Physics and Chemistry (University of Lodz). From 1999 to 2003, I investigated the crystal and molecular structures of new derivatives of *N*,*N*'-substituted phosphonylated thiourea under the supervision of Prof. Maria Bukowska-Strzyżewska from the Technical University of Lodz. Additionally, I worked on crystal structures of compounds synthesized in the Department of Bioinorganic Chemistry (Medical University of Lodz) in cooperation with a group led by Prof. Justyn Ochocki. Also, together with a the Head of the Crystallography and Crystal Chemistry Group (University of Lodz) Prof. Sławomir Grabowski, I started performing theoretical calculations with a subsequent application of the Quantum Theory of Atoms in Molecules[1] for model complexes of thiourea. This was my first experience of analyzing theoretical electron density distribution. The topological analysis of hydrogen bonds allowed me to gain a deeper insight into the studied electronic structures; this was a significant achievement in my structural studies, which had, until then, only been based on an Independent Atom Model (IAM). In 2006, we published an independent project [H1] considering the nature of non-conventional F–H···F–C interactions.

However, information about electronic structure can be obtained not only from the theoretical calculations, but also from the aspherical model structures derived from X-ray experiments. My subsequent post-doctoral position in a group headed by Prof. Peter Luger introduced me to work with experimental electron density distribution, and I contributed to a number of research projects conducted by the group. A publication [H2] considering two modifications of tripetide L-Ala-L-Tyr-L-Ala was my first success in the charge density studies: I performed crystallographic calculations to obtain a multipole model, which I then verified using quantum chemical calculations based on the crystal geometry. I have also actively participated in other electron-density projects[2] [H3,H4]. Despite the lack of a diffractometer at my home laboratory, I was able to continue my electron density studies after my return to Lodz thanks to collaboration with a synchrotron station at Hasylab/DESY in Hamburg (Germany), where I could perform X-ray measurements. The high resolution X-ray data measured there during two projects, of which I was Project Leader, formed the basis of a number or publications, including two of which I submitted for the habilitation procedure [H5, H6]. In article [H5], the weak interactions contributed by π electrons were considered on the basis of the electron density distribution of three (aza)izoinole derivatives. It is worth mentioning that a high-resolution X-ray data set measured at beamline D3 in Hasylab at ultra-low temperature (8K) for methylurea was used in a project [H6]. Most of the crystallographic calculations, including new techniques where the wavefunction is fitted to X-ray data, were performed during the DAAD (Deutscher Akademischer Austauschdienst) fellowship in Georg-August University in Göttingen (Germany). I went on to use these methods for modeling the electron density distribution of difluoroborate dyes[3] [H7] as well as flavanone derivatives [H8]; one unusual aspect of the analysis was that the results were based on the use of low-resolution data. During another DAAD stay in Bremen, I maintained contact with the X-ray experiment and was able to use new techniques in theoretical calculations.

The scientific aim

To summarize, my scientific activity since receiving my PhD in 2003 has focused on experimental and theoretical electron-density studies for small molecules. The central aim of all publications used in the habilitation procedure is to interpret the character of chemical bonding and to gain a deeper insight into the nature of non-covalent interactions.

[H1] Characterization of non-covalent interactions: F–H···F–C hydrogen bonds.

The first article included in the list of habilitation achievements [H1] was inspired by the growing interest in interactions with fluorine atoms. This study analyzes non-conventional hydrogen bonds of the type F–H···F–C, based on quantum chemical calculations. Complexes of hydrogen fluoride as the proton donor and fluoro derivatives of methane, ethene and ethyne as the proton acceptor were taken into account (Fig. 1).

As a strongly electronegative atom, fluorine follows the Pauling definition of hydrogen bonding[4], in that it may act as both a proton donor and a proton acceptor. In literature, the HF molecule is known as a strong proton donor[5] while the structural fragments with C–F are considered weak proton acceptors.[6] The aim of this study was to analyze the properties of F–H···F–C systems, i.e. those containing a strong HF proton donor and a weak C–F proton acceptor. It considered the influence of carbon hybridization on the accepting properties of fluorine, as well as the substituent effect of additional fluorine substituents in hydrocarbons on the characteristics of H-bond interaction.

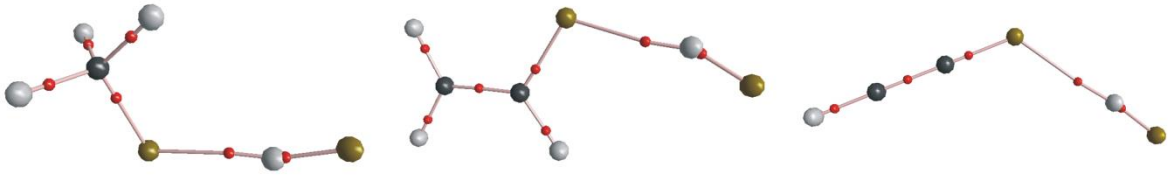

(*a*) (*b*) (*c*)

Figure 1. Molecular graphs of the selected complexes: $H_3CF\cdots HF$ (*a*), $H_2C{=}CHF\cdots HF$ (*b*) and $HC{\equiv}CF\cdots HF$ (*c*).

Methodology: Full geometry optimizations were performed with the use of DFT (Density Functional Theory) and MP2 (Møller-Plesset perturbation theory) methods: B3LYP/6-311++G(d,p), MP2/6-311++G(d,p), MP2/aug-cc-pVDZ. The binding energies of the analyzed complexes were corrected for the basis set superposition error using the counterpoise method.[7] The Quantum Theory of Atoms in Molecules (QTAIM) was applied to characterize bond critical points (bcps), especially those attributed to H···F interaction, the H–F proton donating bond and C–F accepting fragments.

The study found the elongation of the H–F proton-donating bond (hydrogen fluoride) to be in the range 0.001 – 0.01Å following complexation with hydrocarbons. The MP2 calculations found the H–F bond length for the monomer to be 0.925Å, with the H–F proton donating bond for the complex with monofluoromethane was longer (0.935Å). The shortest H–F bond length (0.926Å) was observed for systems with the following acceptors: $F_3CF\cdots HF$, $HC{\equiv}CF\cdots HF$ and $FC{\equiv}CF\cdots HF$. Moreover, the H···F distance corresponds to H–F bond length: the shortest H···F distance (1.740Å) corresponds to the longest H–F bond length interacting with the H_3CF acceptor. Furthermore, different dependencies between energetic and geometrical parameters are observed. As expected, binding energies correlate linearly with H–F proton-donating bond length and H···F proton···acceptor distance. The greatest binding energy was found to be 5.96kcal/mol for $H_3CF\cdots HF$ and corresponds to both the shortest H···F distance and the longest H–F bond length. Excellent agreement was found between energetic and geometrical parameters for the weakest interactions below 1kcal/mol, since such binding energies occur for F_3CF, $HC{\equiv}CF$ and $FC{\equiv}CF$ acceptors.

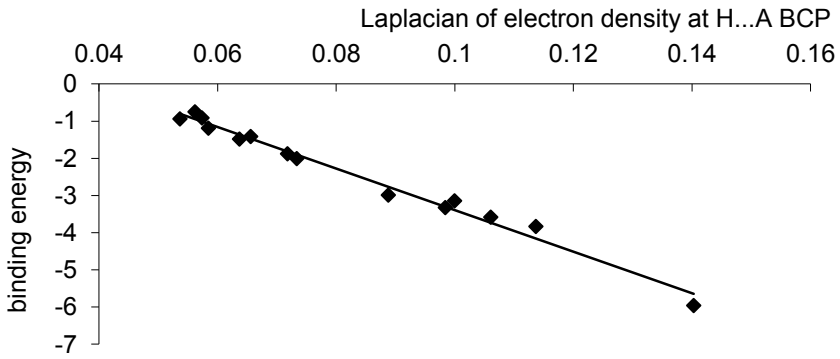

$y = -55.865x + 2.1943$ $R=0.992$

Figure 2. The relationship between the Laplacian of the electron density at H···F bcp (in au) and the binding energy (in kcal/mol) (at the MP2/aug-cc-pVDZ level of theory).

As noted by other studies,[8] good relationships were found between binding energy and topological parameters. Figure 2 shows the linear correlation between binding energy and the Laplacian of the electron density at the H···F bond critical point. One can conclude that the quite strong linear relationships, with a correlation coefficient around 1, may be the result of the same HF molecule being used as the proton donor for all investigated complexes and the related species of acceptors. It is worth mentioning that all trends and relationships mentioned above for geometrical, topological and energetic parameters found at the MP2/aug-cc-pVDZ level of theory are fulfilled for all levels of approximation applied in this study: B3LYP/6-311++G(d,p), MP2/6-311++G(d,p); however, it is difficult to compare the considered methods.

The most important observations and conclusions:

- Intermolecular F—H···F—C interactions are rather weak H-bonds; the binding energies of the investigated complexes range from 0.82 kcal/mol to 5.96 kcal/mol.
- Hybridization of C-atom connected with the fluorine acceptor influences the strength of F—H···F—C interactions: the strength of the hydrogen bond increases in the following order $C(sp) \rightarrow C(sp^2) \rightarrow C(sp^3)$.
- The substituent effect in accepting molecules: additional fluorine substituents decrease the binding energies in the following order for fluoromethane derivatives as acceptors: $H_3C–F$, $H_2FC–F$, $HF_2C–F$, $F_3C–F$. Similar tendencies are observed for fluoro derivatives of ethene and ethyne; however, in the former case, the binding energies depend also on the position of the fluorine substituent.

Application:

The last decade has seen immense growth of interest in fluoroorganic chemistry due to the wide practical applications of fluorinated compounds in pharmaceutics, the agrochemical industry[9] and Medicine.[10] This has been accompanied by a dramatic increase in the number of structural reports highlighting the significance of weak interactions associated with the presence of so-called 'organic fluorine' in a molecule.[11] In this context, the results presented in publication [H1] provide a valuable insight into the interactions of F–H···F–C and other closely-related contacts.

[H2] Reproducibility and transferability of bonding and atomic properties: charge density study of tripeptide L-Ala-L-Tyr-L-Ala.

Article [H2] is a part of a series of systematic comparative studies of the charge density of tripeptides of the type L-Ala-Xxx-L-Ala, where Xxx represented one of the 20 naturally-occurring amino acids.[12] An earlier article was based on a corresponding study of the reference tripeptide L-Ala-L-Ala-L-Ala.[12a] Study [H2] considers two crystalline modifications of the tripeptide L-Ala-L-Tyr-L-Ala, which were obtained by two methods: Crystallization from water by slow evaporation of the solvent, which yielded crystals of modification (**1**) [$C_{15}H_{21}N_3O_5 \times 2.634\ H_2O$] (Figure 3*a*), and by the diffusion of ethanol into an aqueous solution of the tripeptide, which resulted in the formation of crystals of modification (**2**) [$C_{15}H_{21}N_3O_5 \times C_2H_5OH$] (Figure 3*b*). Crystal structures of both modifications were published separately based on low-order X-ray data sets. In [H2], two crystalline modifications of the tripeptide L-Ala-L-Tyr-L-Ala were the subject of experimental charge density studies based on high resolution X-ray data collected at ultra-low temperatures of 9K (**1**) and 20K (**2**), respectively. The experimental multipole models were compared with theoretical models constructed from the experimental geometries.

The existence of the tripeptide L-Ala-L-Tyr-L-Ala in two crystal lattices with similar molecular structures (and even similar intermolecular interactions, in most cases) offered a valuable opportunity to examine the reproducibility of the charge density of the given molecule in different crystal structures with comparable crystalline environments (water *versus* ethanol). In addition, experiment was performed under different conditions: synchrotron radiation, T=9K *versus* Mo*K*α, *T*=20K. Similar aspects of the reproducibility of topological parameters had been studied earlier for a hexapeptide and strychnine under different experimental conditions.[13] Concerning transferability, the atomic and bond topological properties of the main peptide chain were compared with those of tri-L-alanine, thereby verifying the influence of the individual central amino acid residues (tyrosine/alanine) on the topology of oligopeptide main chains. A summary of the L-Ala-Xxx-L-Ala project was published in 2009.[12d]

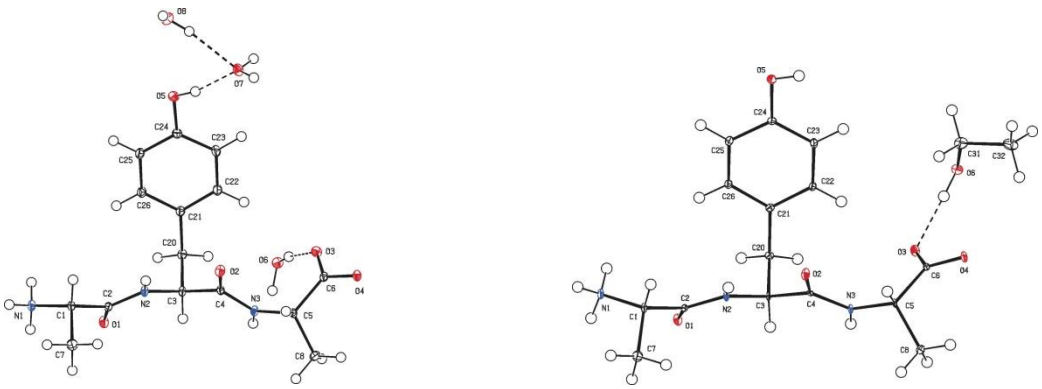

(*a*) (*b*)

Figure 3. Molecular structures of two modifications of the tripeptide L-Ala-L-Tyr-L-Ala: hydrate (*a*) and solvate C_2H_5OH (*b*).

Intermolecular interactions observed in the crystal lattices of both investigated modifications were characterized quantitatively and qualitatively based on topological criteria and by mapping the charge density distribution on the Hirshfeld surface (ρ_{mol}/ρ_{cryt}=0.5) (Fig. 4*a*). The site and the strength of intermolecular interactions can easily be identified by a color code of electron density mapped on the surface. The images were generated with MOLISO software,[14] which also allows the rotation of the image on a graphical interface, so that all close intermolecular interactions and their implications on electron density rearrangement can be visualized in three dimensions. Figure 4*a* was used as the cover for Organic & Biomolecular Chemistry.

The hydrogen bond energies calculated with the relation given by Espinosa et al. [E_{HB}=25300×exp(-3.6×(H···A)) kJ/mol][15] indicated that the hydroxyl group of the tyrosyl residue forms the strongest H-bonds in both modifications of L-Ala-L-Tyr-L-Ala while the weakest interactions are the type of N_{pep}–H···O_{pep}.

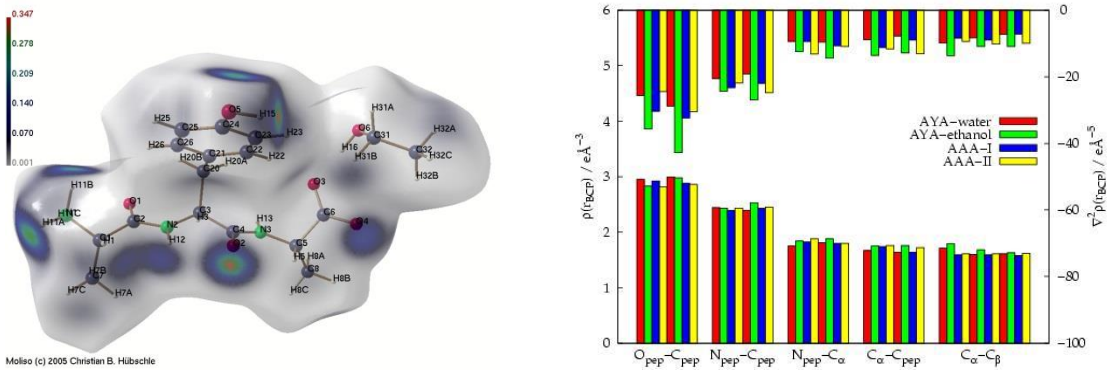

(*a*) (*b*)

Figure 4. The Hirshfeld surface for the ethanol modification (**2**) calculated from experimental charge density. Crystal electron density (in eÅ^{-3}) mapped by a colour code onto this surface (*a*). Comparison of the bond topological properties (ρ_{bcp} and $\nabla^2\rho_{bcp}$) of different types of bonds within the main peptide chain for both modifications of L-Ala-L-Tyr-L-Ala and two independent molecules of L-Ala-L-Ala-L-Ala (*b*).

The most important observations and conclusions:

- The electron densities of all 23 non-hydrogen bonds differ between two modifications of L-Ala-L-Tyr-L-Ala within an mean value of 0.07eÅ^{-3} whereas the Laplacians differ by 4.9eÅ^{-5}. Hence, taking into account the previous literature results, average spreads in the range of 0.1eÅ^{-3} for ρ_{bcp} and 3-5 eÅ^{-5} for $\nabla^2\rho_{bcp}$ seem to indicate the reproducibility of these quantities from charge density determinations under different experimental conditions and different crystal lattices if the intermolecular interactions are comparable.
- The experimental and theoretical bond topological properties can be regarded as reliable in the same ranges given above for reproducibility. However, significant differences in Laplacian values were observed for polar C–O bonds, due to the limited flexibility of the radial functions in the multipole model.
- Reproducibility of integrated atomic properties in the peptide bond regions is in the range of 0.8Å^3 for atomic volumes (V_{001}) and 0.1e for charges (Q_{001}).
- Transferability of bond and atomic properties in the peptide main chain is in the same range as given above regarding the reproducibility of both modifications of L-Ala-L-Tyr-L-Ala and two independent molecules of L-Ala-L-Ala-L-Ala (Figure 4*b*).

Application:

Since replacing the central amino acid L-Ala by L-Tyr appears to have no influence on the topological or the atomic properties of the bonds, our results verify Bader's concept of the transferability of chemically equivalent submolecular fragments. These findings also experimentally confirm the nearest/next nearest approximation and support the development of data bases for electron density modeling of macromolecules.

The high resolution X-ray data sets of both modifications of the tripeptide L-Ala-L-Tyr-L-Ala were successfully used in an alternative refinement of electron density distribution using the Maximum Entropy Method (MEM).[16]

[H3] Characterization of covalent bonds and non-covalent interactions: a study of the experimental charge density of sucrose.

Although sugar is consumed daily in its crystalline state, the first simple X-ray analysis on sucrose was published in 1952, and the structures were determined at currently accepted accuracy as recently as the 1970s.[17] In 2012, the high-pressure structure of the (+)-sucrose polymorph was determined.[18] As sucrose and most other carbohydrates were considered as large molecules, for many years, experimental charge density studies were carried out only in exceptional cases due to the time-consuming nature of high-resolution X-ray diffraction experiments. However, technical and methodological developments have since reduced the time required for the charge density analysis of sucrose. The experimental multipole model (Fig. 5) was compared with the theoretical model obtained by single-point density functional calculations at the B3LYP/6-311++G(3df, 3pd) level of theory.

The aim of the study [H3] was to analyze the atomic and bond topological properties of sucrose based on its experimental charge density obtained at 20 K. The quantitative description of electronic structure of sucrose was based on the topological analysis of two types of covalent bonds: O–C and C–C. For example, for the non-polar C–C single bonds, a good agreement was observed between the experimental and the theoretical topological properties. For these bonds, the experimental and theoretical electron density values at the bcp were found to differ by 0.04*e*Å^{-3} (average), while the corresponding difference for the Laplacians was 0.2*e*Å^{-5}.

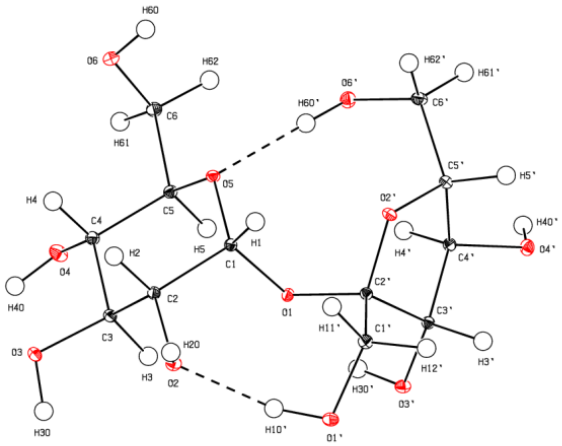

Figure 5. Molecular structure of sucrose.

A QTAIM analysis of charge density distribution shed more light on the topological properties of noncovalent intra- and intermolecular interactions and afforded a deeper insight into the strength of these interactions. In the asymmetric unit of sucrose, nine O–H···O hydrogen bonds were found and analyzed: two of which were found to be intramolecular interactions while the rest were intermolecular. The influences of these interactions on the electronic structure are illustrated quantitatively in the static deformation density maps. For example, it was found that the electron density cloud referring to the lone-pair electrons of the accepting O2 atom is shifted more toward H10' than those of O5 toward H60'. A detailed comparison of the geometrical, topological and energetic parameters for these two intermolecular interactions indicates that the O1–'H10'···O2 H-bond is stronger than the corresponding O6'–H60'···O5 interaction. The weakest interactions are intermolecular hydrogen bonds involved in the bifurcated donor system: O4–H40···O2' and O4–H40···O6. For all hydrogen bonds of the type O–H···O, existing in the crystal structure of sucrose, the electron density (ρ_{bcp}), associated Laplacian ($\nabla^2\rho_{bcp}$) and the positive curvature (λ_3) values were plotted versus the H···O distances. The literature relations are also shown for comparison.[19]

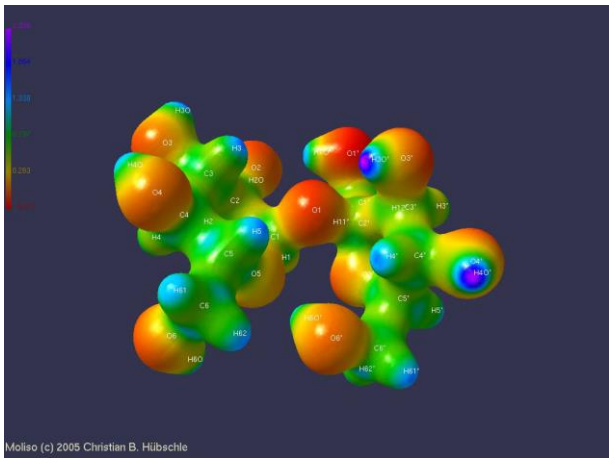

Figure 6. Experimental electrostatic potential mapped according to a colour code on the electron density isosurface of sucrose (ρ=0.5eÅ^{-3}).

The electrostatic potential (EP) was also considered when studying the charge density of sucrose, since EP is very helpful for determining the reactive behavior of a chemical system. The negative regions can be regarded as nucleophilic centers, whereas regions with positive EP are potential electrophilic sites. The electrostatic potential of sucrose was calculated from high-resolution experimental data according to Su and Coppens[20] and is represented on the electron density isosurface. Figure 6 shows noticeable negative electrostatic potential around the oxygen atoms and positive regions around the hydrogen atoms. Moreover, it can be seen that the hydrogens from the hydroxyl groups involved in hydrogen bonding have a stronger positive EP than the hydrogen atoms at the carbon atoms not involved in interactions.

The most important observations and conclusions:

- The study of the experimental charge density distribution of sucrose allowed the quantitative atomic, bonding and non-bonding properties to be determined.
- The influence of anomeric carbon atoms, the endocyclic O—C bonds (O5—C1 in the pyranosyl ring and O2'–C2' in the furasnosyl ring), to the anomeric carbon atoms are characterized by 10-20% higher electron density than the bonds O5—C5 and O2'—C5'.

Application:

In 2009, the multipole model of sucrose (presented in study [H3]) based on the high resolution X-ray diffraction data (d=0,43Å, T=20K) was compared with an alternative model refined using the Invariom method[21] (X-ray data cut at d=0.85Å, T=20K).[22] A comparative study of both models revealed good agreement of the bond topological and atomic integrated properties, thereby verifying the reliability of Invariom formalism.

[H4] Characterization of non-covalent interactions: intermolecular interactions of $C_{60}(CF_3)_{12}$.

In study [H4], the charge density of the fullerene $C_{60}(CF_3)_{12}$ was determined based on a high-resolution X-ray data set measured at 20K. The $C_{60}(CF_3)_{12}$ molecule exhibits high-point symmetry S_6 which is also adopted in the crystal. Its molecular and crystal structures are associated with unusual physical properties such as low solubility and volatility.[23] The study focused on the qualitative and quantitative examination of intermolecular interactions between the polar non-trifluoromethylated hexagons. It was found that in the crystal lattice, the molecules are separated by a distance of only 3.311Å (Fig. 7*a*) in the *c*-direction. This particular intermolecular arrangement in $C_{60}(CF_3)_{12}$ was considered as stabilizing the structure with respect to its dissolution or evaporation processes.

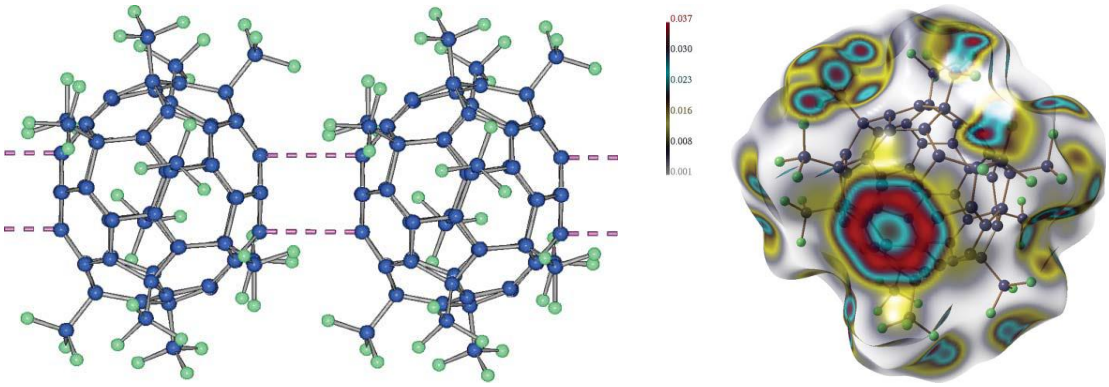

(*a*) (*b*)

Figure 7. A scheme of intermolecular interaction between hexagons of adjacent molecules of $C_{60}(CF_3)_{12}$ (*a*). Hirshfeld surface of $C_{60}(CF_3)_{12}$ with the crystal electron density mapped onto it (in eÅ^{-3}) (*b*).

The most important observations and conclusions:

- Strong shrinkage was found for the cage-carbon atoms carrying the CF_3 group, but an even greater decrease in volume was seen for the *exo*-cage carbons of the CF_3 group, leading to an exceptionally small volume, V_{001}C(exo-F_3)=3,24(4) Å^3, accompanied by a strong positive charge, Q=1.69e, to compensate for most of the negative charges of the three fluorine atoms.
- The substituent effect: the above mentioned observation confirmed that the strong negative charge associated with the fluorine substituents is almost entirely compensated by those of their parent carbons, depending on the number of fluorines. Based on the theoretical electron density distribution of the CF_4 molecule, the smallest carbon atom volume of 1.89Å^3 was also found to have a simultaneous increase of positive charge to 2.52*e*.
- Topological analysis of the intermolecular region yielded bond, ring and cage critical points with very low electron density values of 0.002-0.004eÅ^{-3}. More pronounced is the crystal electron density concentration visible on the Hirshfeld surface (Fig. 7*b*) which clearly indicates weak intermolecular hexagon-hexagon interaction.

[H5] Characterization of non-covalent interactions: analysis of weak intermolecular interactions on the basis of experimental and theoretical electron-density distribution for three (aza)isoindole derivatives.

A combined experimental and theoretical study of three isoindole derivatives was made on the basis of a topological analysis of their electron-density distributions. Since the analyzed structures possess a variety of weak intermolecular interactions with the contribution of π-electrons, they represent a subject of special interest and are discussed in detail. To better characterize these interactions, knowledge of the electron delocalization effect within the investigated (aza)isoindole molecules was required. Hence the HOMA index,[24] delocalization index, [25] and bond ellipticity [26] for phenyl groups and (aza)isoindole moieties were examined to confirm the presence of a delocalized π-system. Using AIM theory, the weak intermolecular C–H···π, π···π and H···H interactions were characterized and compared with conventional of O–H···O type hydrogen bonds, as well as weak C–H···O interactions. Interactions with π-systems were conveniently expressed by close contacts between individual atoms of these systems: C–H···(C)π and (C,N)π···(C,N)π, respectively.

A topological analysis revealed that the values of electron density at the bond critical point of H···C(π) contacts are slightly lower than for (C)H···O type. The differences are more pronounced with regard to local energy density values (*G*, *V* and *H*), which are about half those found for (C)H···O interactions. For the long weak interactions the sum of the distances d_1 and d_2 (distances from bcp to atom 1 and 2, respectively) is longer (0.03-0.05Å) than the direct geometrical distance *d*, whereas the total bond path length *l* is significantly longer than *d* up to 0.4Å. For comparison, the difference between direct bond distance and the bond path length is only 0.01-0.02Å for strained and curved banana C–O and C–C bonds in epoxides.[27] Despite the visible differences in bond distances, for C···C and C···N contacts representing stacking π···π interactions, the same dependencies were found for H···C(π) contacts, indicating that both interaction types with π-electrons are of similar strength. It is worth mentioning that for the analyzed contacts, both the topological parameters and the energetic parameters, which themselves also depend on topological ones, are higher if derived by the experimental multiple model. This can be interpreted as the interactions being stronger in the crystal, which could be attributed to a mutual strengthening of the intermolecular interactions by the complete pattern of interactions. The geometrical effects should be excluded, since experimental geometries were used for single-point calculations of the dimers, and the direct contact distances are the same. The QTAIM analysis performed for intermolecular H···H contacts, for which the existence of bond critical points and bond paths was confirmed, showed that the topological parameters were in the same range as those of the π-electron interactions; however, they were slightly weaker than literature values.[28]

Moreover, the identification of individual types of contacts and a reader-friendly graphical representation was made possible by mapping the electron-density distribution (Fig. 8*a*), electrostatic potential (Fig. 8*b*) and the geometric function d_{norm} (Fig. 8*c*) on the Hirshfeld surface of azaisoindole derivatives I-III. The geometric function d_{norm} used in the CrystalExplorer[29] software is a ratio including the distances of any surface point to the nearest interior (d_i) and exterior (d_e) atom and the van der Waals radii of the atoms themselves (r_i^{vdW}).[30] If the values of d_i and d_e for any Hirshfeld surface point are plotted against each other, so called *fingerprint plots* are generated (Fig. 8*d*). By reducing the fingerprint to plots including a chosen contact (atomtype1···atomtype2), it is possible to allocate the features to these types of contacts and obtain the percentage surface coverage for the individual interaction types. For analyzed crystal structures I-III, the highest contributions (up to 50%) were found for H···H contacts, due to the small van der Waals radius of the hydrogen atom. Although there were many H···H contacts, only a few of them are the shortest.

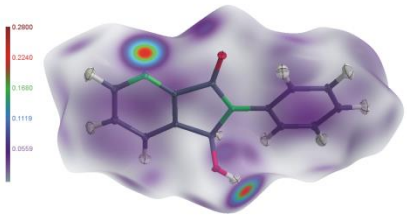

(*a*)

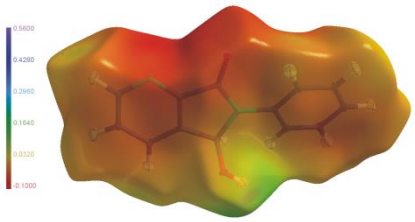

(*b*)

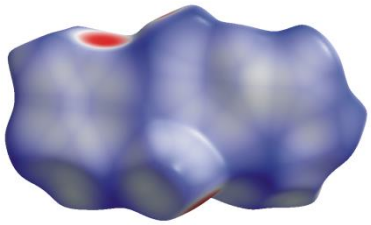

(*c*)

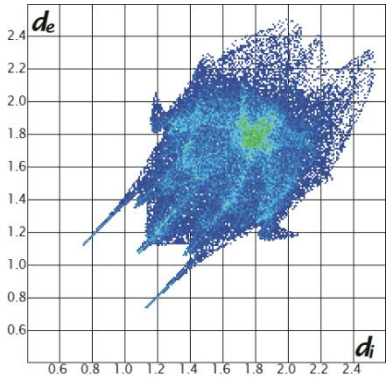

(*d*)

Figure 8. Hirshfeld surface of azaisoindole derivative (II) with the total experimental aspherical electron density (in eÅ^{-3}) mapped onto it according to the multipole model (*a*); with the experimental electrostatic potential (in eÅ^{-1}) mapped onto it (*b*) (both MolecoolQT representations).[31] Hirshfeld surface of azaisoindole derivative (II) with the geometric function d_{norm} mapped onto it (*c*) and corresponding fingerprint plot (*d*) (Crystal Explorer representation).

The most important observations and conclusions:

- Based on the comparative study of experimental and theoretical electron density distribution of three (aza)isoindole derivatives the weak intermolecular contacts of C–H···π, π···π and H···H types were characterized. Interactions with a contribution of delocalized π-electrons were described on the basis of close contacts between individual atoms of these systems: H···C(π) and C,N(π)···C,N(π).
- Hirshfeld surface analysis using the d_{norm} function allows all close contacts to be to identified and distinguished from each other, whereas mapping the crystal electron density or experimental electrostatic potential onto the Hirshfeld surfaces clearly indicates the covalent or electrostatic contribution of stronger interactions.
- As the nature of the interaction can be fundamentally influenced by subtle differences in density (as shown by the comparison of experiment *versus* theory in this study), differentiation between the attractive and repulsive types of H···H interaction should always be done carefully.

Application:

Conclusions from this work might be further used in experimental and theoretical charge-density studies[32] on weak intermolecular interactions, which are responsible for supramolecular structures.

[H6] Characterization of chemical bonding: a comparison of the multipole model with the basis-set model derived by X-ray wavefunction refinement.

The aim of the study [H6] to compare the basis-set model obtained from X-ray wavefunction refinement (XWR) with the multipole model.[33] At present, the multipole model is the most popular for use in experimental electron-density studies. In multipole refinement, the electron density in the crystal is approximated as a sum of atomic density functions, which are allowed to be aspherical.[34] The multiple expansion parameters describe the asphericity of atoms, which are called pseudoatoms. Instead of modelling pseudoatoms, we can obtain aspherical atomic density functions from quantum mechanical calculations. Hirshfeld-Atom Refinement (HAR)[35] is based on the assumption that the crystal is composed of a single molecule, whose electron density can be approximated by quantum mechanical calculations of isolated molecules. The Hirshfeld partitioning technique[36] is then used to carve up the molecular density into aspherical atomic density functions called Hirshfeld atoms. The obtained non-spherical atoms are used as scattering factors in a least-squares refinement of structure parameters. The wavefunction obtained in the HAR method can be subsequently used in an X-ray constrained wavefunction fitting procedure (XCW).[37] The XCW approach combines the least-squares and variational concepts. The wavefunction is yielded by the simultaneous minimization of the agreement statistic (χ^2) and wavefunction energy, supported by introducing a Lagrange multiplier λ; however, this wavefunction is constrained to the experimental data within the acceptable experimental error bounds. In 2012, the combination of two mentioned techniques, HAR and XCW, was called X-ray wavefunction refinement.[33]

Study [H6] presents a comparison of the following aspherical models of three urea derivatives on the basis of the high resolution data sets: the multipole model as a reference model (known in literature), the basis-set model of HAR, with and without the presence of cluster of charges and dipoles (+/-) around the central molecule simulating the crystal environment, and finally the XWR-model, formally obtained after X-ray constrained wavefunction fitting: the second step of XWR (Fig. 9). Both density functional calculations, HAR and XWR, were performed using the BLYP[38] functional in combination with the Dunning cc-pVDZ and cc-pVTZ[39] basis sets using Tonto[40] software.

In order to compare the investigated structural models, the following aspects were discussed: final figure of merit, the residual and deformation density maps, geometries of molecules, the topological parameters (ρ_{bcp}, $\nabla^2\rho_{bcp}$) at the bond critical points and integrated atomic properties (V_{001}, N_{001}, Q) according to the AIM partitioning scheme.

The residual electron density maps obtained after the HAR and XCW steps are essentially identical and featureless in comparison with those from multipole refinements. In the latter case, some characteristics are present, e.g. a minimum at most atomic nucleus positions. Therefore, the basis-set models seem to be the better quality (Fig. 10).

As expected, the agreement statistic (χ^2) found the fitting accuracy in the HAR and XCW methods to be better, since its changes after constraint refinement are much more variable than those of the *R* factors.

The most important observations and conclusions:

- The figures of merit (*R*, R_w, *S*, χ^2) obtained using the cc-pVTZ basis-set are the best; however, comparable results can be obtained using a double-zeta basis set. Hence, the cc-pVDZ basis set is recommended for larger systems.
- An advantage of the HAR method is that it effectively reproduces the bond distances to hydrogen atoms from neutron diffraction, and at the same time allows the positional parameters to be refined freely.
- The HAR model is more accurate than the multipole one: the standard deviations of non-hydrogen bond lengths after Hirshfeld atom refinement are systematically improved in most cases when compared with the multipole refinement.

- Since X-ray wavefunction refinement based on the geometry obtained by Hirshfeld atom refinement provides a high quality electron-density model, this two-step procedure is recommended for crystallographers interested in charge-density studies.

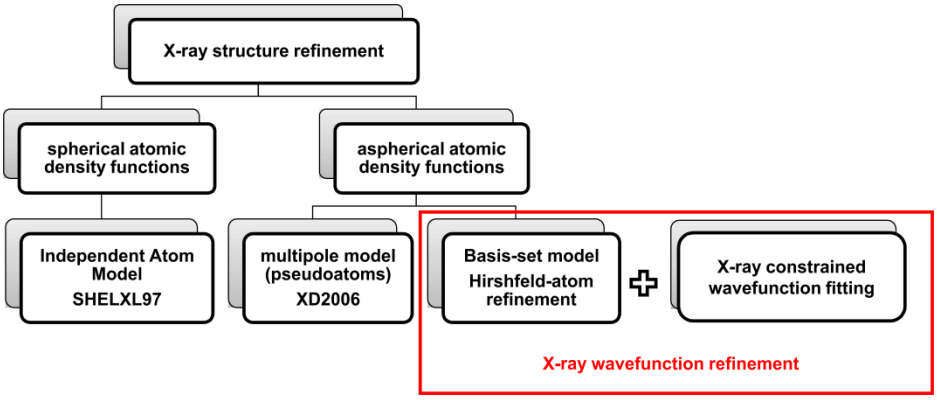

Figure 9. An overview of the different structure models and their relationship to each other.

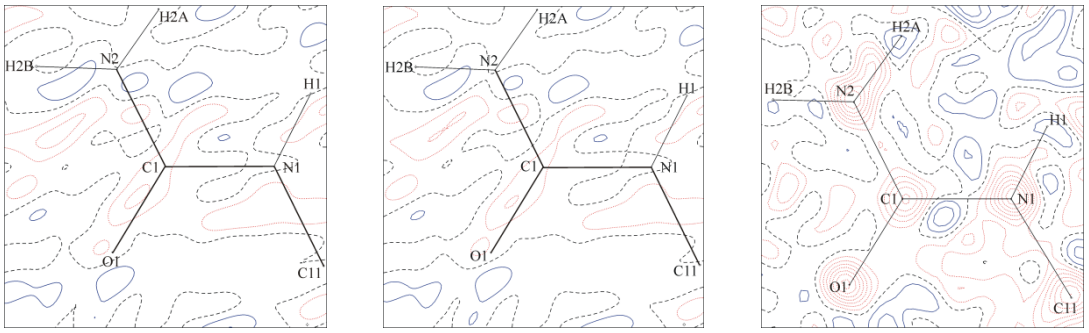

(*a*) (*b*) (*c*)

Figure 10. The residual electron-density maps for *N*-methylurea after Hirshfeld atom refinement with a cluster of charges (+/-) (*a*), after X-ray constrained wavefunction fitting (*b*) and after multipole refinement (*c*).

Application:

Hirshfeld atom refinement provides information about molecular structure. This method can be successfully used for standard X-ray data since a high-resolution data set is not required[3] [H7,H8]. Despite several technical limitations, for example, disordered structures and structures with more than one independent molecule in the asymmetric unit are excluded from refinement, the basis-set model may be soon be competitive with the Independent atom model (IAM).

[H7] Characterization of chemical bonding: Electron Localizability Indicator (ELI-D) derived from X–ray wavefunction refinement.

Difluoroborate dyes are interesting because of their fluorescent properties.[41] Despite the many structural studies performed on these compounds, especially those concerning spectroscopic data or theoretical calculations,[42] the first detailed analysis of chemical bonding of the type B–X, where X=N,O,F, within the kernel N–BF_2–O, was published as recently as 2013.[3] Research project [H7] is a continuation of the mentioned analysis: the electron structures of two difluoroborate derivatives [2-benzoylmethylenequinoline difluoroborate (**1**) and 2-(4-trifluoromethyl)benzoylmethylenequinoline difluoroborate (**2**)], obtained by X-ray wavefunction refinement using low resolution datasets, were compared with the experimental basis-set model of a third derivative [salicylidene-4-isopropylaniline difluoroborate (**3**)].

The nature of the N–B and O–B bonds within these structures was analyzed by a set of topological and integrated real-space bonding indicators (RSBIs) utilizing two space partitioning schemes: the Quantum Theory of Atoms In Molecules (QTAIM), which divides space into basins of atoms, and the Electron Localizability Indicator (ELI-D),[43] which divides the space by paired electrons. A combination of these two methods provides quantitative information about the strength and character of a bond. It is also very well suited for the simple detection of weak atomic interactions and lone pair regions.

The most commonly considered RSBI include the electron density at the bond critical point (ρ_{bcp}) and its corresponding Laplacian ($\nabla^2\rho_{bcp}$), the bond ellipticity (ε), the delocalization index (δ), the ratios of the kinetic and total energy density over ρ_{bcp} (G/ρ_{bcp} and H/ρ_{bcp})[5a] (the degree of ionicity and degree of covalency, respectively). Moreover the volume (V_{001}^{ELI}) and the electron population (ELI_{pop}) of the ELI-D basin are determined using ELI-D. The Raub-Jansen index (*RJI*)[44] is calculated by combining AIM and ELI-D analysis: an ELI-D bonding basin is divided into the contributions of the AIM atoms which constitute the bond. Simply, the RJI gives the absolute or relative numbers of electrons associated with an ELI-D basin within an AIM atom.

In [H7] ELI-D properties were derived for fully optimized gas-phase structures as well as for structures with the geometry taken from the crystals (model sp). The most important achievement is that the ELI-D analysis was performed based on the X-ray contrained wavefunction derived from XWR method (Figure 11). This is only the third example of the X-ray contrained wavefunction being successfully used in ELI-D calculations.[45]

To gain a deeper insight into the nature of the dative N–B bond with the associated O–B interaction, 10 theoretical model structures were also proposed. By doing this, it was possible to determine the substituent effect caused by F/H exchange. Additionally, for the reference conjugated model and its derivatives (F_2/FH/H_2) the analysis of real-space bonding indicators was completed by the Fermi orbitals approach[46] (Figure 12*d*-*e*).

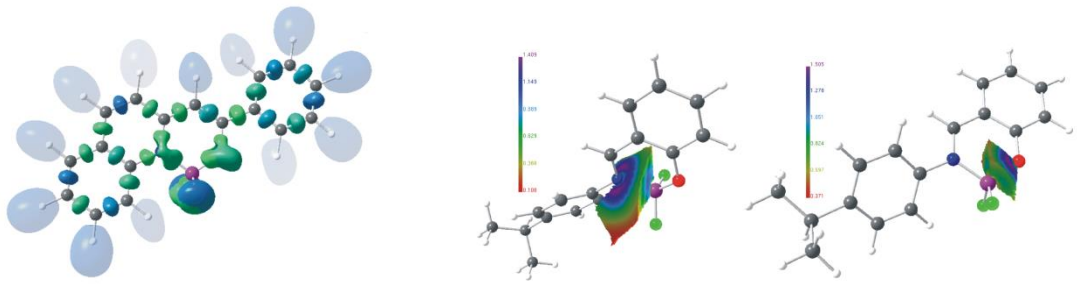

(*a*) (*b*) (*c*)

Figure 11. Experimental ELI-D localization domain representation of compound (**1**) (Y = 1.50) (*a*); ELI-D distributions mapped on bonding basins of N–B (*b*) and O–B (*c*) for compound (**3**).

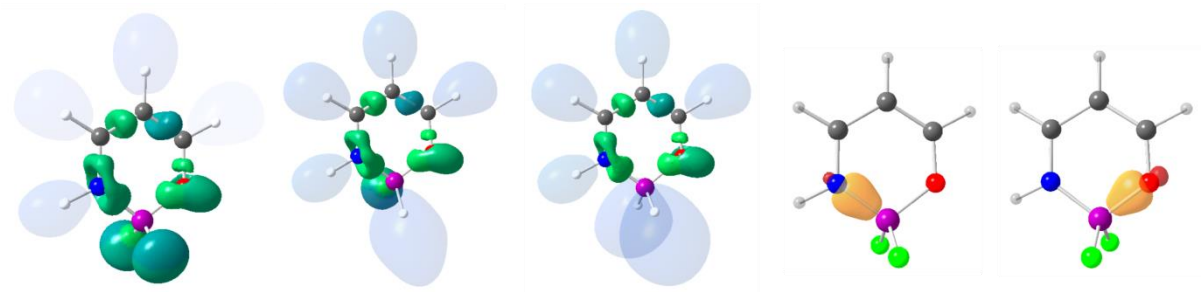

(*a*) (*b*) (*c*) (*d*) (*e*)

Figure 12. Theoretical ELI-D localization domain representations for a reference model structure with two fluorine atoms (*a*), one fluorine atom and one hydrogen atom (*b*) and two hydrogen atoms (*c*) (Y=1.40). The figure presents the Fermi orbitals attributed to the N–B (*d*) and O–B (*e*) bonds; these orbitals are for the QTAIM basin of B atom, more precisely its QTAIM atomic basin. Orbitals are drawn for a reference model structure.

Each atomic basin of B, N, O, F (or H) within an N–BF_2–O fragment is characterized by five Fermi orbitals with an occupation higher than 0.1: a core orbital, orbitals attributed to chemical bonds, or orbitals representing lone pairs. Low occupation of orbitals integrated for the B atom (0.2 – 0.3) indicates that the orbitals do not penetrate the boron basin. Similarly, low delocalization indices indicate low covalent contribution in the bonds with the B atom.

The most important observations and conclusions:

- In real crystal structures **1 – 3,** the spatial arrangement of the aromatic benzene ring (structures **1 – 2** versus structure **3**) has no influence on the bonding situation within the analyzed fragments. Conjugation was found to have a similar effect for small model structures.
- In real compounds **1 – 3** and model structures with the N–BF_2–O fragment, the N–B bond is essentially described as dative, and the O–B bond as strongly polar. However, the similar values found for many real-space bonding indicators may indicate that these bonds have a polar-dative character.
- Considering the effect of the stepwise substitution of the fluorine atoms by hydrogen atoms in model compounds including the N–B–O fragment, the N–B and O–B bond lengths become somewhat longer, leading to a slightly greater degree of iconicity and higher bond ellipticities. The trend is more pronounced for the O–B bond, which is more sensitive to changes in the substitution pattern of the boron atom.
- An analysis of Fermi orbitals revealed that the fluorine atoms share electrons with other fluorine atoms, as well as nitrogen and oxygen atoms, resulting in delocalization indices around 0.16, emphasizing the long distant interactions of the F atom. The strong polar character of the F–B bond stands in remarkable contrast to the pronounced distant sharing of the F atoms.
- Similarly for the fluorine atoms, the hydrogen atoms bonded to the boron atom demonstrate quite high distant electron sharing comparable to their close sharing with the boron atom.
- The influence of conjugation was investigated by a comparison of a conjugated reference model with an aliphatic six-membered ring system. In the latter, the N–B bond is significantly elongated with a much shorter O–B bond. At the same time, the effective charge of the N atom decreases while the charge of the O atom increases. The nitrogen atom (together with the attached hydrogen) dispenses electrons to the C–C–C–O chain.

Application:

A detailed understanding of the electron properties of the investigated systems may be important in the design of new structures and for future applications as fluorescent dyes.

Moreover, the proposed set of real-space bonding indicators, using QTAIM and ELI-D methods, combined with Fermi orbital analysis allow the nature of chemical bonding to be described from a different point of view.

[H8] Characterization of chemical bonding: electron structure of synthetic flavanone derivatives.

Since flavonoids show potential anticancer, antioxidant and antibacterial properties, their application in medicine and pharmacy has aroused growing interest. Furthermore, beneficial synergistic interactions have been found between flavonoids and metal ions. Complexes with nitrogen-containing ligands are also the subject of intensive biological evaluation to find less toxic and more selective anticancer agents.[47]

Article [H8] uses structural studies to determine the crystal structures of synthetic flavanone derivative (**1**) and its palladium(II) complex (**2**). (Fig. 13). For both compounds, the independent atom model (IAM) was refined, and geometry optimization for investigated molecules was performed at BLYP/cc-pVTZ. The same level of theory was used in X-ray wavefunction refinement for compound (**1**) on the basis of a low resolution X-ray dataset. For an experimental XWR model of (**1**) and theoretical models of (**1**) and (**2**), an analysis of bond situation was performed using a set of real-space bonding indicators. Similarly to previous study, the Quantum Theory of Atoms in Molecules and the Electron Localizability Indicator were used.

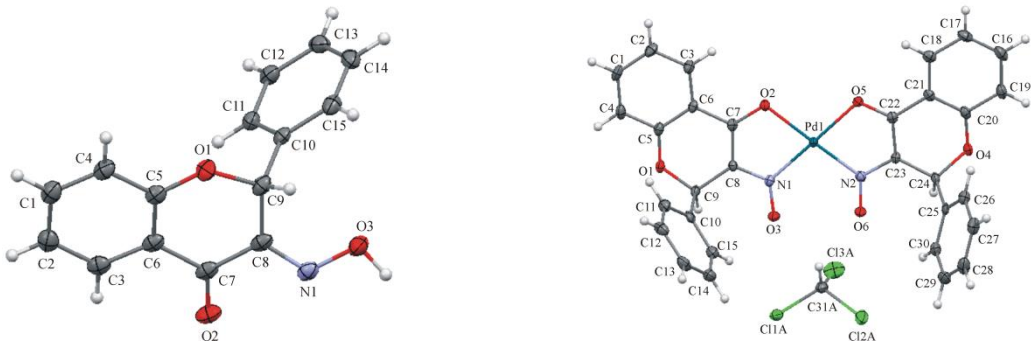

(*a*) (*b*)

Figure 13. Molecular structure of flavanone ligand (**1**) (*a*) and its palladium(II) complex (**2**) (*b*).

Molecule (**1**) consists of a benzene ring condensed with a 6-membered heterocyclic ring, which carries a phenyl ring and =NOH group. The system of two condensed rings is essentially planar. In the complex structure, two flavanone ligands are in anionic form. The Pd(II) center of (**2**) is tetracoordinated in bis-bidendate fashion via two nitrogen atoms (N1 and N2) and two oxygen atoms (O2 and O5), thus the geometry is distorted square planar. The 6-membered heterocyclic rings adopt a skew-boat conformation. The asymmetry parameters C_2=3.9(3)° and C_2=1.2(3)° imply the existence of the pseudo-twofold axis crossing the midpoints of O1–C9 (ligand 1) and O4–C24 (ligand 2) bonds, respectively.

In Pd(II) complex structure (**2**), the structural fragments within the flavanone moieties O2-C7-C8-N1-O3 (ligand 1) and O5-C22-C23-N2-O6 (ligand 2) clearly contain delocalized π-systems. A considerable shortening of bond lengths C7–C8/C22–C23 and N1–O3/N2–O6 in comparison to the free ligand structure of (**1**) is accompanied by the significant lengthening of bond distances O2–C7/O5–C22 and N1–C8/N2–C23. Geometrical changes are reflected in such topological parameters as electron density and associated Laplacian at the bond critical point of the considered bonds (electron density values at bcp increase and decrease when the distance is shortened and lengthened, respectively). Furthermore, these trends are confirmed by the bond ellipticity and the delocalization index. Additionally, an analysis of lone-pair basins of nitrogen and oxygen atoms was performed using the ELI-D technique.

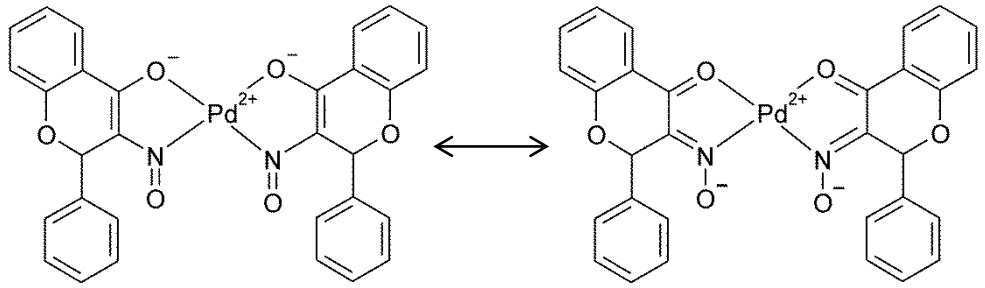

form 1 form 2

Figure 14. Two resonance forms of Pd(II) complex (**2**).

The most important observations and conclusions:

- In the crystal structure of Pd(II) complex (**2**), the monoanionic forms of the flavanone ligands are arranged in a *cis*-configuration around the metal centre.
- For the studied Pd(II) complex (**2**), two resonance forms are possible (Fig. 14). Structural studies indicate that form 1 seems to be dominant in the solid state of (**2**), and π-delocalization is observed within the O–C–C–N–O flavanone moieties.
- Pd–O interactions have a fairly strong ionic nature, whereas Pd–N bonds have more of a polar character.

Summary [H1 – H8]

The analysis of the electron density distribution on the basis of X-ray data and/or quantum chemical calculations [H1–H8] has shed light on the electronic structure of the investigated systems, including information about lone pairs, and the characterization of chemical bonds and weak no-covalent interactions. The combination of QTAIM and ELI-D techniques allowed the number of real-space bonding indicators to be expanded, which will prove helpful in the interpretation of character of bonds and the nature of intermolecular interactions.

X-ray wavefunction refinement (XWR) consists of two methods: Hirshfeld Atom Refinement (HAR) and X-ray constrained wavefunction fitting (XCW). However, neither are commonly used in crystallography. Article [H6] was one of the first papers to use these methods in structural studies since the methodology was originally published (2008, 1998-2002). Only a few groups, mainly those associated with the authors, currently promote these relatively new research techniques.

In the last two projects [H7, H8] the Electron Localizability Indicator (ELI-D) method plays a crucial role. While a typical ELI-D analysis is performed on the basis of theoretical calculations, the ELI-D properties were exclusively extracted from the X-ray constrained wavefunction derived from conventional low-resolution X-ray diffraction data in [H7, H8].

4.4. Other research achievements

My other scientific achievements have been published as 27 articles from peer-reviewed journals listed in Journal Citation Reports as well as seven structural reports in Acta Crystallographica (Section E). Besides the electron density studies, including these submitted in the habilitation procedure, I have contributed as a crystallographer in many interdisciplinary projects in which I typically determined the crystal and molecular structures of complexes based on ions such as palladium(II), platinum(II), ruthenium(II) and silver(I). I am currently responsible for the X-ray diffraction analysis as a part of a study financed by a National Science Centre grant (2015-2018), the beneficiary being a team headed by Professor Justyn Ochocki from the Medical University of Lodz; the title is: Silver(I) complexes of imidazole and pyridine derivatives – synthesis, structural characterization, antimicrobial and cytotoxic activity.

Earlier, our joint scientific-research achievements have received three awards from the Rector of the Medical University of Lodz and once by the Minister for Health: all being team awards for a cycle of publications. In addition, I have also received three awards from the Rector of the University of Lodz, these also being team awards for a cycle of publications.

Literature

[1] R. F. W. Bader, Atoms in Molecules. A Quantum Theory, Oxford University Press, New York, 1990.
[2] S. Grabowsky, T. Pfeuffer, L. Chęcińska, M. Weber, W. Morgenroth, P. Luger, T. Schirmeister (2007). Eur. J. Org. Chem. (2007). 2759-2768.
[3] A. Zakrzewska, E. Kolehmainen, A. Valkonen, E. Haapaniemi, K. Rissanen, L. Chęcińska, B. Ośmiałowski (2013). J. Phys. Chem. A, 117, 252-256.
[4] L. Pauling, The Nature of the Chemical Bond, Ithaca, NY: Cornell University Press, Ithaca, New York, third edition, 1960.
[5] (a) E. Espinosa & E. Molins (2002). *J. Chem. Phys*.,117, 5529-5542; (b). M. J. Frisch, J. E. del Bene, J. S. Binkley & H. F. Schafaer (1986). *J. Chem. Phys*., 84, 2279-2289.
[6] (a) I. Hyla-Kryspin, G. Haufe & S. Grimme (2004). *Chem. Eur. J*., 10, 3411-3422; (b) J. L. Alonso, S. Antolínez, S. Blanco, A. Lesarri, J. C. López & W. Caminati (2004). *J. Am. Chem. Soc.*, 126, 3244-3249;
[7] S. F. Boys & F. Bernardi (1970). *Mol. Phys*., 19, 553-566.
[8] (a) L. F. Pacios (2005). *Struct. Chem*., 16, 223-241; (b) S. J. Grabowski (2004). *J. Phys. Org. Chem*., 17, 18-31; (c) S. J. Grabowski (2001). *J. Phys. Chem*., A105, 10739-10746.
[9] (a) H. Roesky (2011). *Nat. Chem*., 2, 240; (b) K. Muller, C. Faeh & F. Diederich (2007). *Science*, 317, 1881−1886; (c) S. Purser, P. R. Moore, S. Swallow & V. Gouverneur (2008). *Chem. Soc. Rev*., 37, 320−330; (d) W. K. Hagmann (2008). *J. Med. Chem*., 51, 4359−4369; (e) K. L. Kirk (2008). *Org. Proc. Res. Dev*., 12, 305−321; (f) P. Jeschke (2010). *Pest Manag. Sci*., 66, 10−27; (g) D. O'Hagan (2010). *J. Fluorine Chem*., 131, 1071−1081.
[10] A. Tressaud & G. Haufe, Fluorine and Health: Molecular Imaging, Biomedical Materials and Pharmaceuticals ; Elsevier: Amsterdam, 2008.
[11] (a) D. Chopra (2012). Cryst. Growth Des., 12, 541−546; (b) H.-J. Schneider (2012). *Chem. Sci*., 3, 1381-1394; (c) P. Panini & D. Chopra (2012). *CrystEngComm*, 14, 1972–1989; (d) T. S. Thakur, M. T. Kirchner, D. Bläser, R. Boese & G. R. Desiraju (2010). *CrystEngComm*, 12, 2079–2085.
[12] (a) E. Rödel, M. Messerschmidt, B. Dittrich & P. Luger (2006). *Org. Biomol. Chem*., 4, 475-481; (b) D. Förster, A. Wagner, C. B. Hübschle, C. Paulmann & P. Luger (2006). *Z. Naturforsch. B*, 62, 696-704; (c) R. Kalinowski, B. Dittrich, C. B. Hübschle, C. Paulmann & P. Luger (2007). *Acta Cryst*., B63, 753-767; (d) S. Grabowsky, R. Kalinowski, M. Weber, D. Förster, C. Paulmann & P. Luger (2009). *Acta Cryst*., B65, 488-491.
[13] (a) B. Dittrich, T. Koritsánszky, M. Grosche, W. Scherer, R. Flaig, A. Wagner, H.-G. Krane, H. Kessler, C. Riemer, A. M. M. Schreurs & P. Luger (2002). *Acta Cryst*., B58, 721-727; (b) M. Messerschmidt, S. Scheins & P. Luger (2005). *Acta Cryst*., B61, 115-121.
[14] C. B. Hübschle & P. Luger (2006). *J. Appl. Cryst*., 39, 901-904.
[15] E. Espinosa, E. Mollins & C. Lecomte (1998). *Chem Phys. Lett*., 285, 170-173.
[16] J. Netzel & S. van Smaalen (2009). Acta Cryst., B65, 624-638.
[17] (a) C. A. Beevers, T. R. R. McDonald J. H. Robertson & F. Stern (1952). *Acta Cryst*., 5, 689-690; (b) G. M. Brown & H. A. Levy (1963). *Science*, 141,921-923; (c) G. M. Brown & H. A. Levy (1973). *Acta Cryst*., B29, 790-797; (d) J. C. Hanson, L. C. Sieker & L. H. Jensen (1973). *Acta Cryst*., B29, 797-808.
[18] E. Patyk, J. Skumiel, M. Podsiadło & A. Katrusiak (2012). *Angew. Chem. Int. Ed*., 57, 2146-2150.
[19] E. Espinosa, M. Souhassou, H. Lachekar & C. Lecomte (1999). *Acta Cryst*., B55, 563-572.
[20] Z. Su & P. Coppens (1992). *Acta Cryst*., A48, 188-197.
[21] B. Dittrich T. Koritsánszky & P. Luger (2004). Angew. Chem. Int. Ed., 43, 2718-2721.
[22] B. Dittrich, M. Weber, R. Kalinowski, S. Grabowsky, C. B. Hübschle & P. Luger (2009). *Acta Cryst*., B65, 749-756.
[23] S. I. Troyanov, A. Dimitrov & E. Kemnitz (2006). *Angew. Chem. Int. Ed*., 45, 1971-1974.
[24] T. M. Krygowski (1993). *J. Chem. Inf. Comput. Sci*., 33, 70-78.
[25] (a) R. F. W. Bader & M. E. Stephens (1975). *J. Am. Chem. Soc*., 97, 7391-7399; (b) X. Fradera, M. A. Austen & R. F. W. Bader (1999). *J. Phys. Chem*. *A*, 103, 304-314.
[26] R. F. W. Bader, T. S. Slee, D. Cremer & E. Kraka (1983). *J. Am. Chem. Soc*., 105, 5061–5068.
[27] S. Grabowsky, D. Jayatilaka, S. Mebs & P. Luger (2010). *Chem. Eur. J*., 16, 12818-12821.
[28] (a) S. Mebs, S. Grabowsky, D. Förster, R. Kickbusch, M. Hartl, L. L. Daemen, W. Morhenroth, P. Luger, B. Paulus & D. Lentz (2010). *J. Phys. Chem. A*, 114, 10185-10196; (b) S. Mebs, R. Kalinowski, S. Grabowsky, D. Förster, R. Kickbusch, E. Justus, W. Morhenroth, C. Paulmann, P. Luger, D. Gabel & D. Lentz (2011). *J. Phys. Chem. A*, 115, 1385-1395.
[29] M. A. Spackman & D. Jayatilaka (2009). *CrystEngComm*, 11, 19-32.
[30] J. J. McKinnon, D. Jayatilaka & M. A. Spackman (2007). *Chem. Comm*. 3814-3816.

[31] C. B. Hübschle & B. Dittrich (2011). *J. Appl. Cryst*., 44, 238-240.
[32] (a) M. R. V. Jørgensen, V. R. Hathwar, N. Bindzus, N. Wahlberg, Y.-S. Chen, J. Overgaard & B. B. Iversen (2014). *IUCrJ*, 1, 267-280; (b) D. Chopra (2012). *J. Phys. Chem. A*, 116, 9791-9801.
[33] S. Grabowsky, P. Luger, J. Buschmann, T. Schneider, T. Schirmeister, A. N. Sobolev & D. Jayatilaka (2012). *Angew. Chem. Int. Ed.,* 51, 6776-6780.
[34] N. K. Hansen & P. Coppens (1978). *Acta Cryst*., A34, 909-921.
[35] (a). D. Jayatilaka & B. Dittrich (2008). *Acta Cryst*., A64, 383-393; (b) S.C. Capelli, H.-B. Bűrgi, B. Dittrich, S. Grabowsky & D. Jayatilaka (2014). *IUCrJ*, 361-379.
[36] F. L. Hirshfeld (1977). *Theor. Chim. Acta*, 44, 129-138.
[37] (a) D. Jayatilaka (1998). *Phys. Rev. Lett.,* 64(4), 798-801; (b) D. Jayatilaka & D. J. Grimwood (2001). *Acta Cryst*., A57, 76-86.
[38] (a) A. D. Becke (1988). *Phys. Rev. A: At., Mol., Opt. Phys*., 38, 3098-3100; (b) C. Lee, W. Yang & R. G. Parr (1988). *Phys. Rev*. B, 37, 785-789.
[39] T. H. Dunning (1989). *J. Chem. Phys*., 90, 1007-1023.
[40] D. Jayatilaka & D. J. Grimwood, in *Computational Science - ICCS 2003, Part 4: Tonto, A Fortran Based Object-Oriented System for Quantum Chemistry and Crystallography*, Springer, New York, 2003, 142-151.
[41] I. J. Arroyo, R. Hu, G. Merino, B. Z. Tang, E. Pena-Cabrera (2009). *J. Org. Chem*., 74, 5719-5722.
[42] (a) B. Le Guennic, D. Jacquemin (2015). *Acc. Chem. Res*., 48, 530-537; (b) D. Frath, J. Massue, G. Ulrich, R. Ziessel (2014). *Angew. Chem. Int. Ed*., 53, 2290-2310; (c) S. Chibani, B. Le Guennic, A. Charaf-Eddin, A. D. Laurent, D. Jacquemin (2013). *Chem. Sci*., 4, 1950-1963.
[43] (a) M. Kohout (2004). *Int. J. Quantum Chem*., 97, 651-658; (b) M. Kohout, F. R. Wagner & Y. Grin (2008). *Theor. Chem. Acc*., 119, 413-420.
[44] (a) S. Raub & G. Jansen (2001). *Theor. Chem. Acc*. 106, 223-232; (b) I. Vidal, S. Melchor & J. A. Dobado (2005). *J. Phys. Chem. A*, 109, 7500-7508.
[45] (a) S. Grabowsky, M. Weber, D. Jayatilaka, Y.-S. Chen, M. T. Grabowski, R. Brehme, M. Hesse, T. Schirmeister, P. Luger (2011). *J. Phys*. *Chem A*, 115, 12715-12732; (b) S. Grabowsky, D. Jayatilaka, S. Mebs, P. Luger (2010). *Chem. Eur. J.*, *16*, 12818-12821.
[46] (a) R. Ponec, A. J. Duben (1999). *J. Comput. Chem*., 20, 760-771; (b) R. Ponec (1998). *J. Math. Chem*., 23, 85-103.
[47] (a) M. M. Kasprzak, A. Erxleben & J. Ochocki (2015). *Rsc Advances,* 5*,* 45853-45877; (b)B. Kosmider, R. Osiecka, E. Ciesielska, L. Szmigiero, E. Zyner & J. Ochocki (2004). *Mutation Research-Genetic Toxicology and Environmental Mutagenesis,* 558, 169-179; (c) M. A. Jakupec, M. Galanski & B. K. Keppler (2003). *Rev Physiol. Biochem. Pharmacol.*, 146, 1-53.